Sensors & Actuators: A. Physical 411 (2026) 118418

Contents lists available at ScienceDirect

Sensors and Actuators: A. Physical

journal homepage: www.journals.elsevier.com/sensors-and-actuators-a-physical

A self-powered LC wireless sensing platform based on flexible PVDF film

Heng Li [a,1], Yaojun Yuan [a,1], Donglin Wu [a], Jiaqi Zhang [a], Rui Hu [a], Xuemei Lu [b], Enting Gao [c], Tao Peng [d], Baoqing Nie [a,*]

[a] School of Electronic and Information Engineering, Soochow University, Suzhou, Jiangsu 215006, China
[b] Jiangsu Key Laboratory of Biophotonics, Suzhou City University, Suzhou, Jiangsu 215104, China
[c] School of Electronic and Information Engineering, Suzhou University of Science and Technology, Suzhou, Jiangsu 215009, China
[d] School of Future Science and Engineering, Soochow University, Suzhou, Jiangsu 215222, China

ARTICLE INFO

Keywords:
Piezoelectric effect
Self-power
LC resonator
Wireless sensing

ABSTRACT

Poly (vinylidene fluoride) (PVDF) exhibits great potential in the field of flexible wearable sensors due to its excellent piezoelectric properties and mechanical flexibility. Traditional piezoelectric sensors typically operate in a wired connection mode, which can restrict movement when worn and compromise measurement accuracy. To address these issues, this letter proposes a self-powered inductive-capacitive (LC) wireless sensing platform based on PVDF. The system consists of a PVDF piezoelectric film and a flexible LC resonant circuit, enabling the conversion of low-frequency mechanical signals into high-frequency electrical signals in a wireless transmission mode. The working mechanism integrates the piezoelectric effect of PVDF with magnetic resonance of the LC circuit. When the PVDF film is subjected to mechanical pressure, it bends and generates charges on its upper and lower surfaces. Through contact with the LC circuit, these charges are transferred to the LC resonant tank, which radiates high-frequency electromagnetic pulses. This paper reveals the mechanism coupling the PVDF piezoelectric effect and the LC magnetic resonance by establishing an equivalent circuit model. Experimental results show that the peak-to-peak open-circuit voltage of the proposed sensor is approximately twice that of a triboelectric nanogenerator (TENG) with comparable dimensions. By optimizing the size and structural spacing, the sensor maintains stable signal output and exhibits good mechanical durability in repeated tests. The sensor is used to monitor breathing and joint movements, and it is demonstrated to light up an LED using the mechanical energy of breathing, thereby validating its feasibility and application prospects in wireless, self-powered physiological signal detections.

1. Introduction

As an extension of wireless sensor networks into the field of human body monitoring, body area networks (BANs) are gradually becoming a key technology for areas such as health monitoring, medical rehabilitation, and sports science [1–3]. By deploying sensor nodes on the body surface or inside the body, BANs can acquire physiological and motion signals in real time, providing a data foundation for personalized health management and early disease warning [4,5]. Within such networks, individual sensor nodes typically rely on batteries for power. However, conventional battery-based power supply has significant limitations [6–8]. For example, batteries are bulky, occupying valuable space in wearable devices, thereby restricting device form factors and the user's wearing experience [8,9]. In addition, batteries have limited capacity [10,11]. Once depleted, they require manual replacement or recharging, which not only increase high maintenance costs but may also cause monitoring interruptions. To address these issues, researchers have recently proposed the concept of wireless passive sensor nodes, whose core idea is to achieve both energy harvesting and signal transmission wirelessly, thereby eliminating the dependence on embedded batteries [12–14]. For example, Ho et al. report a battery-free sensor network based on near-field communication (NFC) technology [15]. In this system, multiple battery-free epidermal sensors are attached to the skin surface to monitor various physiological parameters in real time. The energy supply and data communication are provided by smart clothing equipped with NFC coils, and the entire system is controlled via an NFC-enabled smartphone, realizing continuous and imperceptible monitoring. To further reduce system power consumption, minimize

* Corresponding author.
E-mail address: qixinbq@suda.edu.cn (B. Nie).
[1] Heng Li and Yaojun Yuan contribute equally to this work

https://doi.org/10.1016/j.sna.2026.118418
Received 8 May 2026; Received in revised form 12 August 2026; Accepted 27 August 2026
Available online 28 August 2026
0924-4247/© 2026 Published by Elsevier B.V.

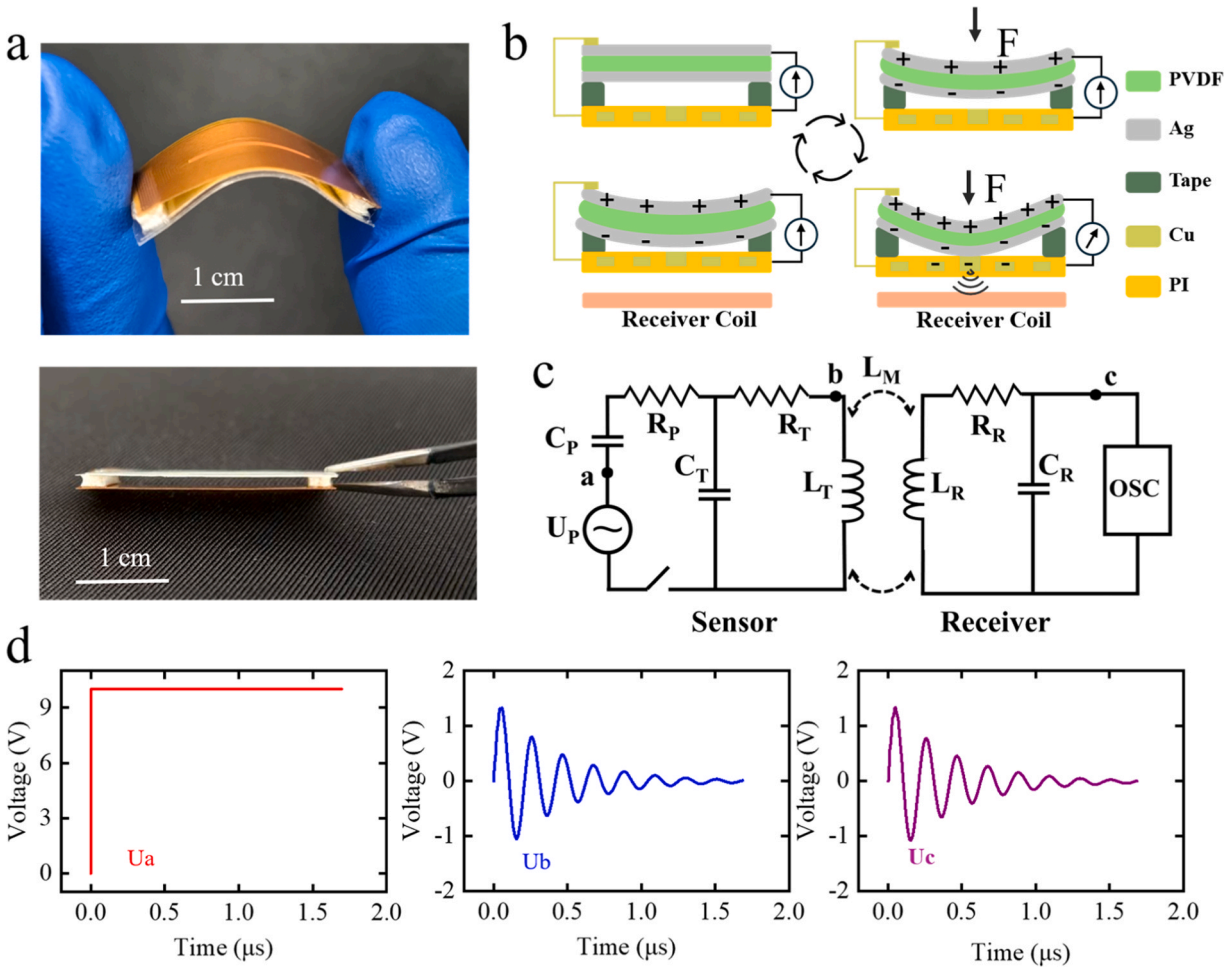


Fig. 1. Working mechanism and equivalent circuit of the PVDF-based self-powered LC wireless sensor. (a) Photographs of the wireless sensor in bent and natural states. (b) Schematic diagram of the sensor's working mechanism under pressure which includes processes: initial state, pressure-induced deformation, charge generation, electrode contact and conduction, LC circuit excitation, pressure release, and device recovery. (c) Equivalent circuit diagram of the system formed by the PVDF-based self-powered wireless sensor and the receiving coil. (d) Circuit simulation on the voltage waveforms at the nodes of *a*, *b* and *c* in the equivalent circuit.

node size, and enhance wearability, chipless and batteryless inductive-capacitive (LC) resonant structures have been introduced into the design of body area network sensors. Such sensors require no built-in chips or batteries and respond to electromagnetic signals solely through inductor-capacitor resonant circuits, greatly reducing node volume and power consumption. These devices are suitable for long-term, unobtrusive, and comfortable wearable integration. Wang et al. propose a battery-free, chipless, and flexible body area network system [16]. This work encodes sensing information through shifts in resonant frequency, achieving physiological signal monitoring while maintaining flexibility and low complexity, thus providing an important technical pathway for a new generation of lightweight, sustainable body area network systems.

In recent years, combining passive wireless transmission schemes with triboelectric nanogenerators (TENGs) to form battery-free, active wireless sensing systems has become an important development direction in the self-powered sensing field [17–19]. Such systems can directly harvest mechanical energy from the environment and convert it into sensing signals, achieving true energy autonomy and wireless information transmission [20]. For example, Han et al. propose a self-powered wireless sensor based on triboelectric-breakdown discharge effect [21]. This system consists of a TENG, an LC resonant humidity-sensitive unit, and a movable breakdown discharge structure. The high-voltage pulses generated by the TENG trigger air-breakdown discharge, which instantly radiates electromagnetic wave signals that are captured and decoded by a remote receiver, thereby enabling passive wireless sensing of humidity information. Furthermore, Zhang et al. report a self-powered wireless sensor network based on a contact-separation mode TENG. This system also integrates a TENG, an LC resonant sensing unit, and a mechanical switch, converting the pulsed voltage output from the TENG into resonant signals that carry sensing information. The sensor achieves real-time wireless transmission over medium-to-long distances, and is successfully applied to self-powered water level monitoring. The above-mentioned works have firmly demonstrated the feasibility of triboelectric-effect-driven LC resonant wireless signal radiation, establishing a relatively mature research paradigm. However, for the other important branch of electromechanical transduction, which is the piezoelectric effect, there has been no report to date on directly driving LC resonant units to radiate electromagnetic waves using piezoelectric materials. Piezoelectric materials offer advantages such as high response sensitivity, stable output, and ease of microfabrication, making them particularly suitable for constructing continuous, low-power sensing nodes [22–24]. Nevertheless, a fundamental question remains unanswered, i.e., if the piezoelectric effect can effectively drive an LC resonator to generate wirelessly detectable signals.

To address this gap, this paper presents the first experimental validation of piezoelectric-driven LC passive wireless sensing, realized through a self-powered LC wireless sensing system based on a poly (vinylidene fluoride) (PVDF) piezoelectric film. The PVDF-LC sensor adopts a multilayer flexible structure, consisting of a PVDF piezoelectric film, a flexible LC resonant layer, and a spacer layer placed between

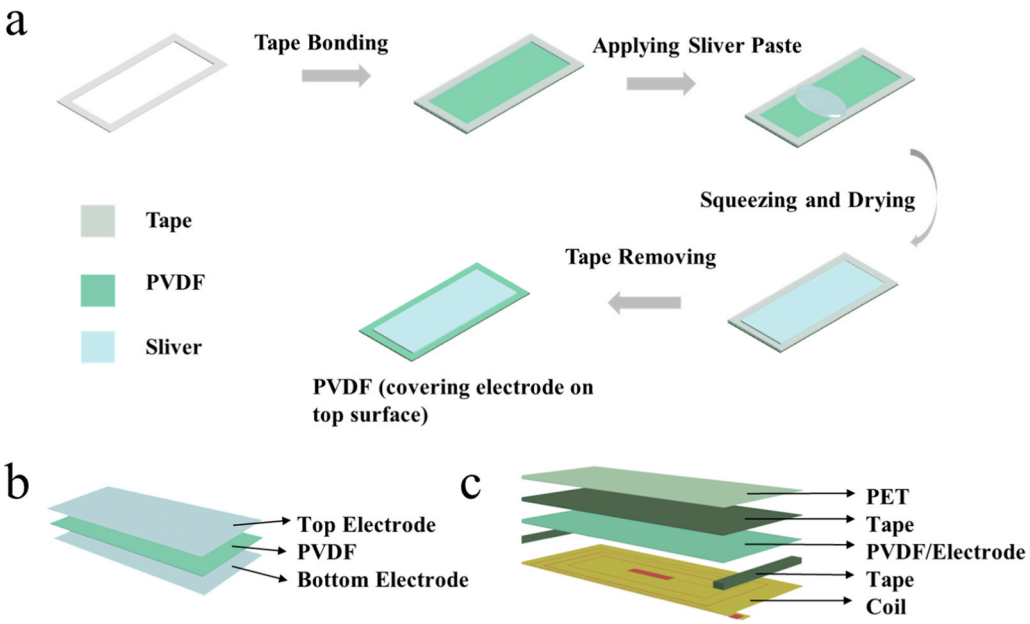


Fig. 2. Fabrication process of the PVDF-based self-powered wireless sensor. (a) Fabrication process of the PVDF electrode layer. (b) Schematic diagram of the PVDF layer with electrode coverage. (c) Schematic diagram of the sensor structural layers.

them. When an external mechanical pressure is applied to the PVDF film, the film generates transient charges due to the piezoelectric effect [25]. Upon contact with the electrodes of the LC resonant layer, these charges excite a damped oscillation in the LC circuit, thereby modulating the low-frequency mechanical signal into a high-frequency electromagnetic resonant signal [26]. The damped oscillation is then wirelessly transmitted and remotely received through magnetic coiling. This design effectively converts the DC-like pulse output of PVDF into a frequency-stable AC carrier, significantly enhancing the signal's anti-interference capability and transmission reliability. This paper investigates the key design parameters affecting sensor performance, including the spacing between the PVDF layer and the LC resonant layer, and the geometry of the inductor coil. To further evaluate the performance advantages of the proposed design, this paper conducts an experimental comparison with a triboelectric nanogenerator (TENG)--based LC wireless sensing scheme. Under the same dimensional conditions, the proposed PVDF-LC sensor achieves a peak-to-peak output voltage of 7.5 V at a transmission distance of 1.5 mm, which is more than twice that of the comparable TENG-based scheme (approximately 3.6 V). In terms of transmission distance, the effective signal of the sensor can be stably transmitted up to 25 mm, far exceeding the limit of approximately 15 mm for the TENG-LC system, demonstrating its remote sensing capability. To validate the utilization, the sensor successfully achieves wireless monitoring of physiological and motion signals such as human respiration rate and joint movement status. These demonstration results indicate that the proposed self-powered LC wireless sensing system with compact structure, battery-free operation, and wearing comfort, exhibits application potential in next-generation wearable health monitoring devices and personalized medical systems.

2. Working principle

2.1. The sensing mechanism of the PVDF-based self-powered wireless sensor

Fig. 1a shows a photograph of the PVDF-based self-powered wireless sensor, demonstrating that the device can withstand large bending deformations. Fig. 1b illustrates the working principle of the PVDF-based self-powered wireless sensor. Under external low-frequency mechanical pressure, the PVDF undergoes reversible deformation. Based on the piezoelectric effect, induced charges opposite polarity are generated on its upper and lower surfaces. When the deformed PVDF comes into contact with the underlying LC resonant antenna, the accumulated charges are injected into the LC resonant circuit, thereby exciting the circuit to produce electromagnetic oscillations at its intrinsic resonant frequency. The oscillatory signal is transmitted to the receiving readout coil through near-field electromagnetic coupling between the coils, manifesting at the receiver as a damped resonant pulse. Upon removal of the pressure, the device returns to its initial state by its own elasticity, ready to respond to the next mechanical excitation.

\

Fig. 1c presents the equivalent circuit model of the system. Previous studies have shown that the PVDF piezoelectric layer can be modeled as a series connection of a piezoelectric voltage U_P and its internal capacitance C_P [27]. The LC resonant unit can be represented as a parallel resonant tank formed by the transmitter inductance L_T and its distributed capacitance C_T. The receiver coil is represented by an inductance L_R in parallel with a distributed capacitance C_R. The internal resistances of the two coils are denoted as R_T and R_R, respectively. R_P represents the contact resistance between the upper PVDF layer and the lower LC resonant antenna at the external contact point. The switch module is used to characterize the contact state between the PVDF and LC resonating layers under applied pressure. When the PVDF deforms under pressure and makes contact with the LC resonant antenna, the switch closes. At that moment, the LC resonant antenna is excited by the transient stimulus and starts to oscillate, generating a resonant signal. When the resistance values of R_P and R_T are small compared to the capacitive and inductive reactance of the LC antenna, the resonant frequency at the transmitting coil port is mainly governed by:

$$f = \frac{1}{2\pi\sqrt{L_T \quad \times \quad (C_P + C_T)}} \tag{1}$$

It is worth noting that if the resistance in the circuit (e.g., contact resistance) increases further, this resonant frequency changes. Furthermore, the open-circuit voltage V_{PVDF} generated by the PVDF is related to its material properties and mechanical loading, and can be approximately expressed as:

$$V_{PVDF} \propto \frac{d \times E \times S}{A \times \varepsilon_{0\times} \varepsilon_r} \tag{2}$$

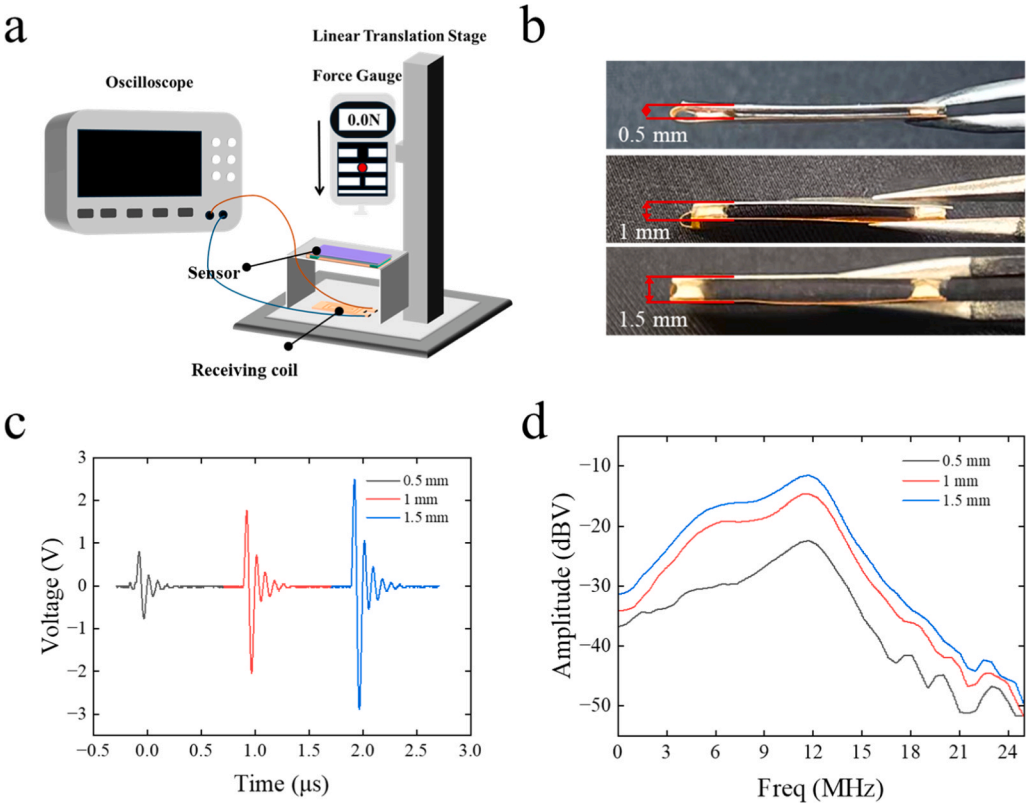


Fig. 3. Performance characterization of the PVDF-based self-powered wireless sensor. (a) Schematic diagram of the measurement setup for sensor performance characterization. (b) PVDF-based self-powered resonant sensors with different spacer layer heights (from top to bottom: 0.5 mm, 1.0 mm, 1.5 mm). (c) Time-domain signals at the receiving coil for different spacer heights. (d) Frequency spectra of the corresponding time-domain signals.

where d is the piezoelectric coefficient of PVDF, E and S are the elastic modulus and the strain of PVDF, A is the effective electrode area, and ε_0 and ε_r are the vacuum permittivity and the relative permittivity of PVDF, respectively.

Fig. 1d shows the time-domain voltage signals from circuit simulation at three nodes (a, b, and c) in the equivalent circuit. When the PVDF is subjected to an external force and comes into contact with the bottom surface, a DC voltage signal U_a is generated at node a. This signal is fed into the LC resonant circuit, exciting a damped oscillatory signal U_b at node b. U_b is then coupled via mutual inductance, inducing a damped oscillatory signal of the same frequency at node c of the receiving coil.

3. Experimental sections

3.1. Materials

PVDF piezoelectric film (thickness: 38 μm, pre-polarized) was purchased from Shenzhen ZhiMeikang Industrial Co., Ltd. Conductive silver paste (E-Solder 3022) was obtained from Suzhou Xinhui High-tech Materials Co., Ltd. Polyethylene terephthalate (PET) film (thickness: 25 μm) and 3 M double-sided adhesive tape (thicknesses: 50 μm and 1 mm) were purchased from Wangda Wang Adhesive Tape Trading Firm, Nanhai District, Foshan City, respectively. The flexible coils were fabricated using a commercial flexible printed circuit (FPC) process, with a polyimide (PI) substrate (thickness: 12.5 μm) and copper traces (thickness: 12 μm). The line width and line spacing were both 100 μm.

3.2. Fabrication process of the sensor

The fabrication process of the PVDF-based self-powered wireless sensor is illustrated in Fig. 2a. First, the pre-polarized PVDF film is fixed on a substrate, and laser-cut masking tapes are covered on its upper and lower surfaces sequentially. Conductive silver paste is then uniformly coated onto both the upper and lower surfaces of the PVDF film. Secondly, the coated film is placed in a drying oven at 70 °C for 60 min to form a stable electrode layer with a uniform thickness (Fig. 2b). The lamination assembly process is shown in Fig. 2c. A 50-μm-thick double-sided adhesive tape and a 25-μm-thick PET substrate are sequentially laminated and adhered onto the upper surface of the PVDF film to form the encapsulation and support structure of the sensor. Finally, two pieces of double-sided adhesive tape with dimensions of 1 mm × 10 mm and a thickness of 1 mm are prepared by laser cutting to serve as the spacer layer. To assemble the final device, the PVDF layer, the spacer layer, and the flexible LC resonant coil layer are bonded together, while the other port lead of the LC coil is brought into contact with the upper electrode of the PVDF and encapsulated.

3.3. Characterization on the sensor performance

The pressure applied to the sensor is generated using a custom-built calibration platform, which includes a linear translation stage (LTS300/M, Thorlabs, Inc.), a force gauge (Mark-10), an impedance analyzer (WK65120B), and a digital oscilloscope (Tektronix MSO64). A constant and controllable pressure excitation is applied to the sensor via the force gauge. The oscillatory signal output from the sensor is wirelessly received by a flexible inductive coil, which is connected to the digital oscilloscope. The voltage signal at the flexible inductive coil is acquired and analyzed using the oscilloscope. To observe the signal envelope, the output of the receiving coil is simultaneously fed into a custom-designed peak detection circuit, and the output signal from this circuit is processed by a data acquisition circuit. The impedance characteristics of the sensor's transmitting coil and the receiving coil are measured using the impedance analyzer.

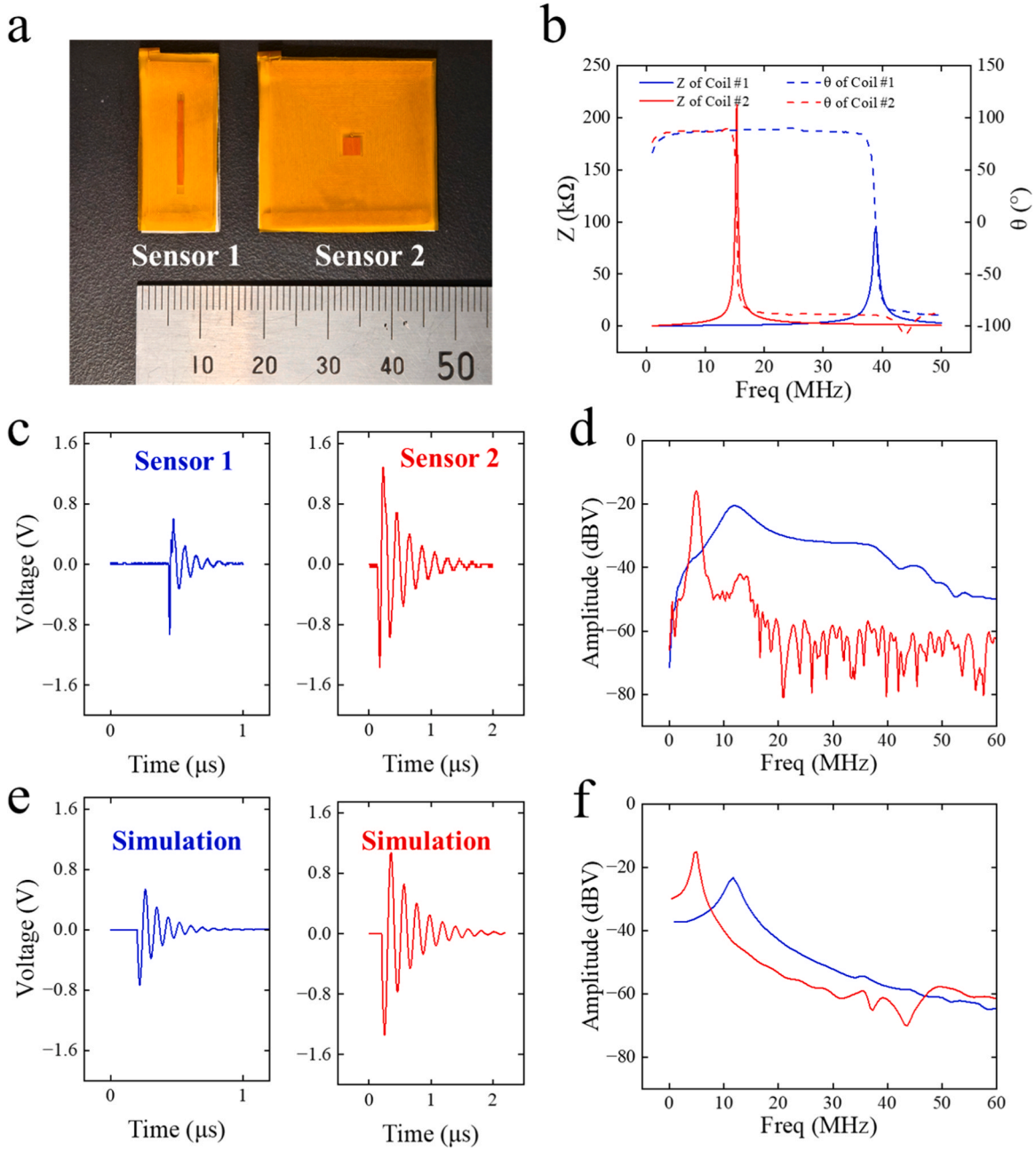


Fig. 4. Effect of different resonant antenna structures on the performance of PVDF wireless sensors. (a) Photographs of two sensors (Sensor 1 and Sensor 2) with different antenna structures. (b) Impedance spectra and phase spectra of the two sensor antennas. For the two sensors, the time-domain waveforms at the receiving coil are shown in (c), and the corresponding frequency-domain waveforms are shown in (d). In the circuit simulation, the time-domain waveforms at the receiving coils of the two sensors are shown in (e), and the corresponding frequency-domain waveforms are shown in (f).

4. Results and discussion

4.1. Influence of design parameters on the sensing performance

The output performance of a sensor depends on the design parameters of its structure. Among these, the spacer layer height serves as a key geometric parameter that directly governs the effective deformation of the piezoelectric layer. According to Eq. (2), the voltage generated by PVDF is proportional to its deformation when it contacts the underlying LC antenna, and this deformation is directly affected by the spacer layer height. Therefore, this study investigates the relationship between the thickness of the intermediate support layer and the voltage across the receiving coil. Fig. 3a illustrates the device calibration setup, which primarily includes a force gauge mounted on a linear stage and an oscilloscope. The external force is applied by the force gauge on the sensor surface, and the voltage output of the receiver coil is recorded by the oscilloscope. Fig. 3b shows photographs of devices with spacer layer thicknesses of 0.5 mm, 1.0 mm, and 1.5 mm, respectively. Under a constant external force of 3 N, the output waveforms of the receiving coil are presented in Fig. 3c. As the spacer layer height increases from 0.5 mm to 1.5 mm, the maximum peak-to-peak oscillating voltage received rises gradually from 1.5 V to 5.3 V. This result is consistent with the prediction: a larger spacer layer height allows PVDF to undergo greater effective deformation (i.e., compression upon contact with the bottom LC antenna) when the PVDF is subjected to pressure. Therefore, more charges accumulate and inject it into the LC resonant tank, leading to a significant increase in the peak output voltage. From the frequency-domain responses for the three cases shown in Fig. 3d, it can be

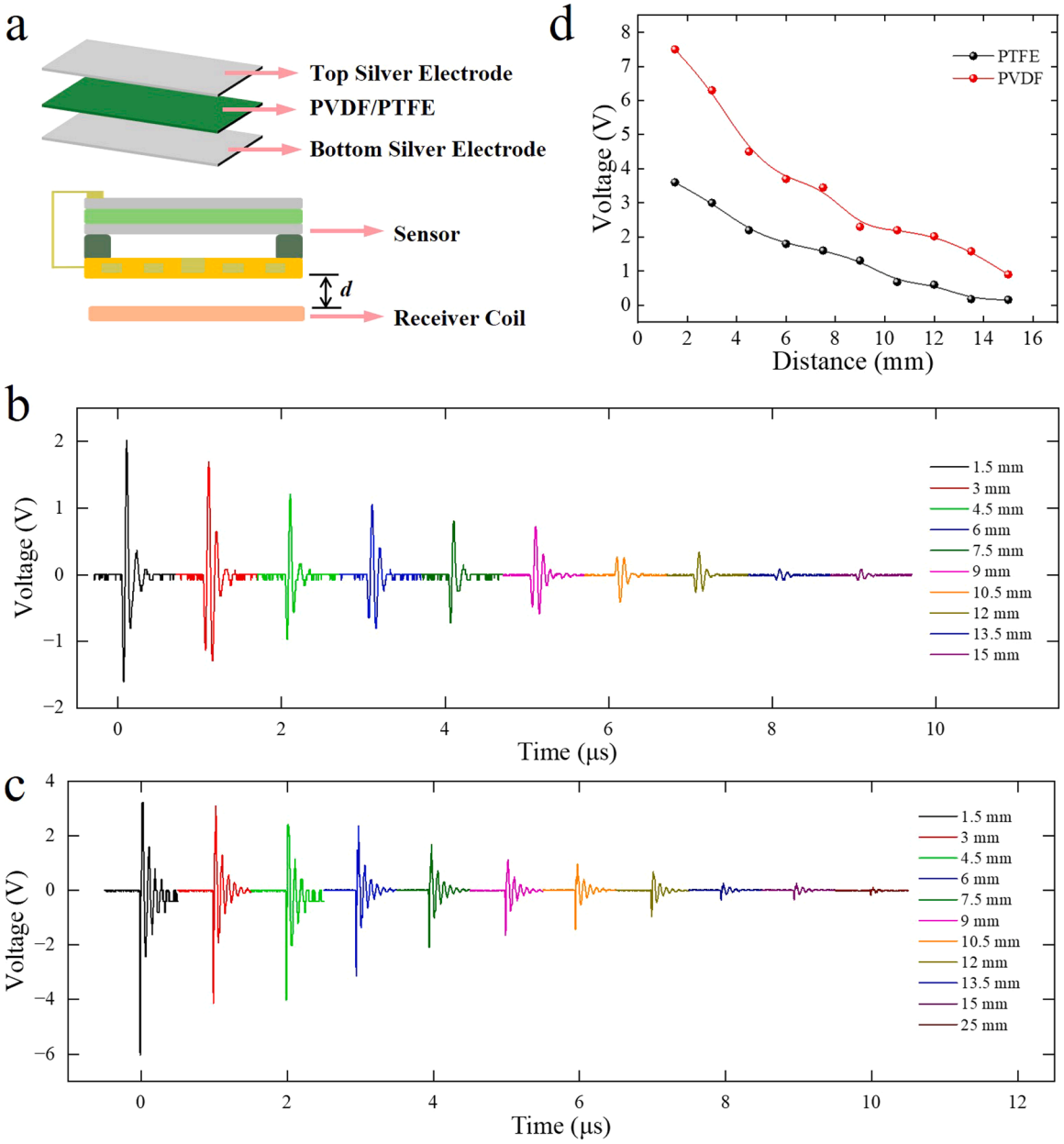


Fig. 5. Performance comparison between PVDF sensor and PTFE sensor. (a) Schematic diagram of the upper-layer structures of the PVDF sensor and the PTFE sensor. (b) Received signal waveforms of the PTFE sensor under vertical distances from the receiving coil ranging from 1.5 mm to 15 mm. (c) Received signal waveforms of the PVDF sensor under vertical distances from the receiving coil ranging from 1.5 mm to 25 mm. (d) Quantitative comparison of the output peak-to-peak voltages of the two sensors over the distance range of 1.5 mm–15 mm.

observed that variations in the spacer layer thickness do not affect the resonant frequency of the system. The center frequencies of all three signals remain stable at 11.9 MHz. Considering both the overall device thickness and output signal magnitude, this study selects the height of 1.0 mm as a compromise that balances compact structure with relatively high output response.

Furthermore, according to the equivalent circuit shown in Fig. 1c, the equivalent inductance L_T and equivalent capacitance C_T of the resonant antenna affect the frequency of the transmitted signal. Therefore, this study investigates the influence of different LC resonant antenna structures on the frequency of the received signal. As shown in Fig. 4a, two sensors with different antenna structures (Sensor 1 and Sensor 2) are fabricated, and their magnitude and phase spectra of the LC resonant antennas/coils are presented in Fig. 4b. The resonant frequencies of Coil 1 and Coil 2 are 38 MHz and 16 MHz, respectively. Under the same applied pressure, the signals emitted by the two sensors exhibit different center frequencies. Figs. 4c and 4d show the time-domain voltage waveforms and the corresponding frequency-domain spectra acquired by the receiving coil, respectively. From the time-domain waveforms, the maximum peak-to-peak voltages of Sensor 1 and Sensor 2 are 1.6 V and 2.8 V, respectively. This phenomenon is primarily attributed to the difference in PVDF dimensions between the two sensors: the PVDF areas of Sensor 1 and Sensor 2 are 25 mm × 10 mm and 25 mm × 25 mm, respectively. According to Eq. (2), under the same deformation, the charge generated is proportional to the PVDF area. The frequency-domain spectra indicate that the center frequencies of the resonant signals emitted by the two sensors are approximately 11.9 MHz and 4.1 MHz, respectively. These results are consistent with the circuit simulation results (Figs. 4e and 4f). Interestingly, when the self-resonant frequency of the resonant coil changes

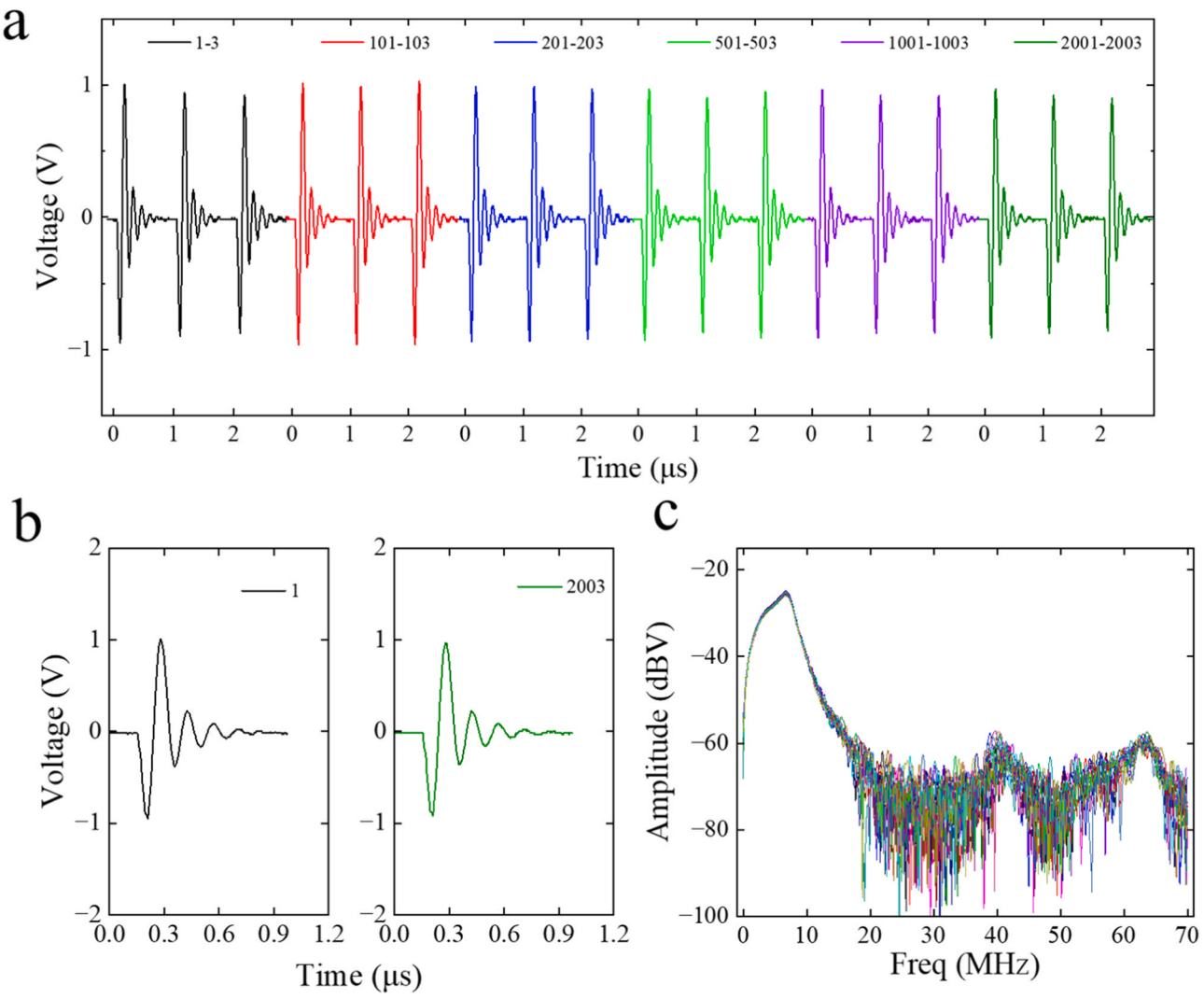


Fig. 6. Repeatability characterization of the PVDF-based self-powered wireless sensor. (a) Time-domain signal at the receiving end under multiple presses on the sensor. (b) Comparison of the output signals under the first and last presses. (c) Frequency-domain spectra of response signals.

from 38 MHz to 16 MHz (Fig. 4b), the frequencies received by the receiving coil changes from 11.9 MHz and 4.1 MHz, respectively. The received frequencies are not equal to the intrinsic frequency of the transmitting antenna, which is mainly because the transmitting coil and the receiving coil are in a strongly coupled state, causing mode splitting of the original single into two new resonant frequencies. One frequency is lower and the other one is higher than the original resonant frequency, denoted as $Freq_{_L}$ and $Freq_{_H}$. Due to the limited bandwidth of the receiving equipment (oscilloscope), the actual detected signal is primarily the low-frequency component. By optimizing these parameters, we can control over the wireless carrier frequency, providing an important theoretical basis for signal differentiation and synchronous monitoring when multiple sensor nodes operate in parallel.

4.2. Comparison between the piezoelectric and triboelectric effects

Furthermore, the proposed sensor operates in a contact-separation mode with the underlying LC resonant antenna, and previous research has indicated that under this mode, triboelectric signals may be included in the output signal [28–30]. To verify this hypothesis, we have conducted a comparative experiment by replacing the piezoelectric material PVDF with polytetrafluoroethylene (PTFE). PTFE is a polymer with pronounced triboelectric properties and is commonly used in studies of the triboelectric effect. Fig. 5a shows schematic diagrams of the upper-layer structures of the two sensors. Both the PVDF and PTFE have dimensions of 10 mm × 25 mm. The LC resonant antenna with a same dimension of 10 mm × 25 mm and has an intrinsic resonant frequency of 38 MHz. Under a constant applied pressure, the transmission distance between the sensor and the receiving coil is varied, and the oscillatory time-domain waveforms of the signals received by the coil for the two sensors are presented in Figs. 5b and 5c. The same phenomena are observed on square-shaped PVDF-based and PTFE-based devices (Figure S1 in the Supplementary Information).

As expected, the PTFE-based sensor, which lacks piezoelectricity, is still able to trigger resonant signals from the LC antenna. At a transmission distance of $d = 1.5$ mm, the maximum peak-to-peak output voltage at the receiving coil reaches 3.6 V. In contrast, under the same conditions, the PVDF-based sensor produced a higher peak-to-peak voltage of 7.5 V. This is probably attributed to the synergistic effect of piezoelectricity and triboelectricity in the PVDF sensor, whereas the PTFE sensor relies solely on the triboelectric effect. In the piezoelectric effect, polarized molecules realign under stress, and the polarization charges are efficiently released into the external circuit. In contrast, the triboelectric effect generates charges through surface charge transfer during contact and separation, a process involving charge separation, interfacial losses, and the gradual establishment of a spatial electric field, which results in a lower amount of effective charge ultimately injected into the LC tank. As the distance d increases, the signal strengths

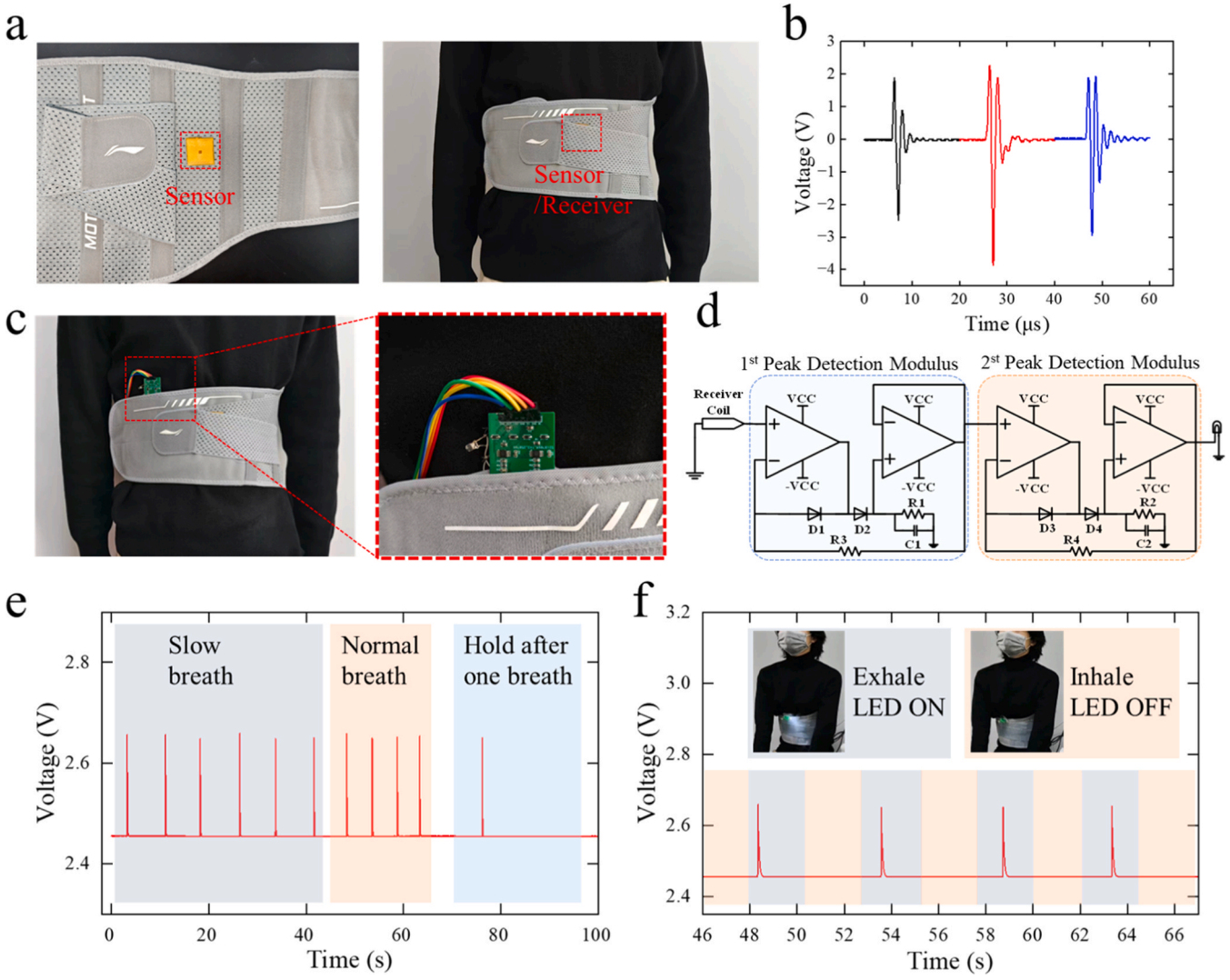


Fig. 7. Application of the PVDF-based self-powered wireless sensor in respiratory signal detection. (a) Photograph showing the placement of the sensor on a waist belt, and a photograph of the waist belt equipped with the sensor worn around the waist. (b) Time-domain waveform of voltage pulses detected at the receiving coil over three respiratory cycles. (c) Photograph of the waist belt (integrated with the sensor and a peak detection circuit) worn around the waist. (d) Block diagram of the signal processing circuit. (e) Voltage waveforms at the LED port under three breathing modes. (f) Voltage waveform at the LED port under the normal breathing mode shown in (e).

of both sensors gradually decrease. At $d = 15$ mm, the output voltage of the PTFE-based sensor drops to 0.14 V, while that of the PVDF-based sensor remains detectable at approximately 0.7 V. When the distance is further increased, the receiving end of the PTFE-based sensor shows almost no significant waveform, whereas the PVDF-based sensor can still output a stable signal of about 200 mV at $d = 25$ mm.

Fig. 5d quantitatively compares the effective transmission distances of the two sensors. Over the range of 1.5 mm to 15 mm, the output voltage of the PVDF-based sensor is consistently higher than that of the PTFE-based sensor. At a distance of 1.5 mm, its output voltage is approximately twice larger than PTFE sensor. It is worth noting that the output signals from PVDF-based devices are generally not purely piezoelectric in nature. As demonstrated by Chen et al. triboelectric signals arising from contact electrification between the polymer and the contacted objects can contribute substantially to the overall output [31]. To verify whether such coexistence exists in our system, we fabricated PVDF layers with opposite polarization directions (forward vs. reverse). The asymmetric output observed between the forward- and reverse-polarity devices (Figure S2 in the Supplementary Information) confirms that the measured signal is indeed a superposition of both effects.

This study has characterized the repeatability of the sensor. The sensor, measuring 25 mm × 25 mm, is subjected to repeated constant-pressure loading for approximately 2000 cycles. At selected cycle numbers, such as the 1st, 100th, 200th, 500th, and so forth, we continuously record the three consecutive pressure cycles immediately following each of these points. As shown in Fig. 6a, the output voltage of the receiving coil exhibits good consistency, with the peak-to-peak voltage per cycle remaining stable within the range of 1.88 V. Fig. 6b presents magnified details of the time-domain signals corresponding to the first and last pressure cycles. The peak-to-peak voltage of the signals remains at 1.88 V, and the time period keep constant around 0.7 μs. From the frequency-domain spectra of the signals for each pressure cycle (Fig. 6c), it can be seen that the resonant frequency remains consistently around 6.6 MHz without significant drift. Furthermore, throughout the entire testing process, the sensor surface maintains good mechanical resilience, with no observable wear or residual deformation. These results collectively demonstrate that the proposed sensor possesses excellent repeatability, stability, and operational durability. In addition, the sensor exhibits a stable output over the temperature ranging from 25 °C to 50 °C and relative humidity from 55% RH to 83% RH (Figure S3 in the Supplementary Information).

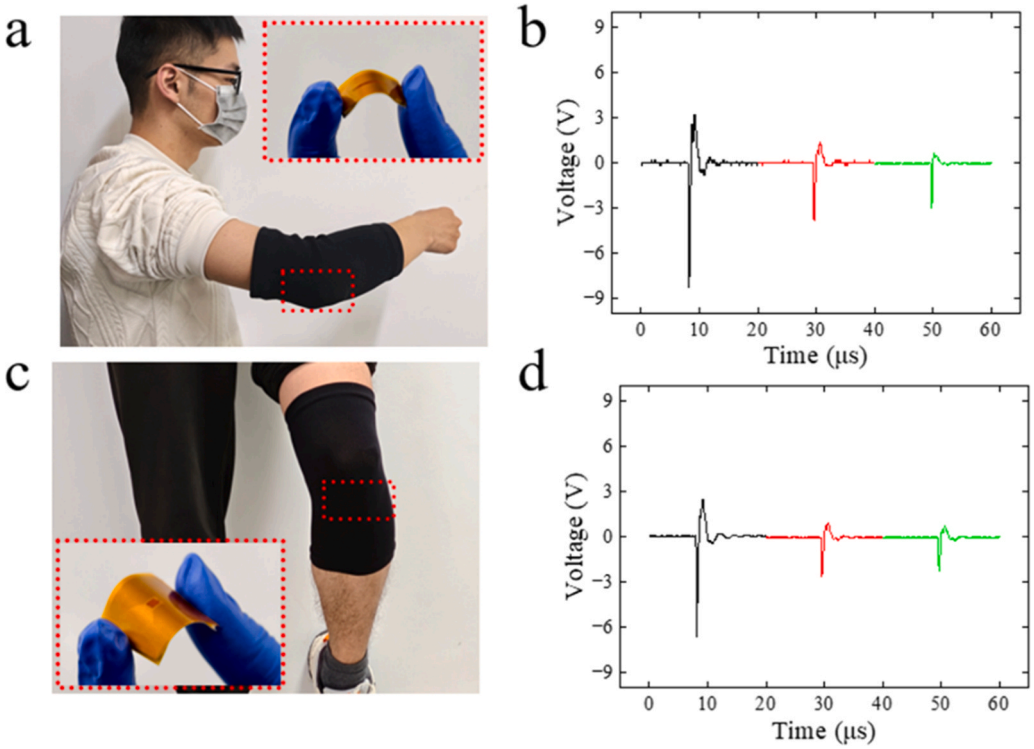


Fig. 8. Application of the PVDF-based self-powered wireless sensor for joint motion detection. (a) Photograph showing the sensor placed on the elbow joint and secured with an elastic band. (b) Three received signals recorded during elbow joint movement monitoring. (c) Photograph showing the sensor placed on the knee and secured with a knee support band. (d) Three received signals recorded during knee joint movement monitoring.

4.3. Application of the PVDF-based sensor in human physiological signal detections

To explore the potential application of self-powered wireless sensors in human physiological signal detection, we have conducted proof-of-principle experiments targeting respiratory rate and joint motion. In respiratory rate monitoring, conventional wired sensors typically require connection to data acquisition equipment via cables, which not only restricts the subject's motion but may also cause discomfort due to cable tugging. Therefore, developing a sensor system that requires no external power supply and enables wireless signal transmission is significance for achieving comfortable, continuous, and unobtrusive respiratory monitoring.

As shown in Fig. 7a, the PVDF-based self-powered wireless sensor is fixed onto a waist belt, and the waist belt is wrapped around the subject's abdomen. The receiving coil is placed at a distance 5 mm directly in front of the sensor. The subject adopts abdominal breathing. During breathing, the periodic expansion and contraction of the abdomen regularly compress the sensor, generating oscillatory signals. These signals are detected by the receiving coil, and the corresponding time-domain waveforms are shown in Fig. 7b. It can be observed that over three slow breathing cycles, the receiving coil captured three clear pulse signals, preliminarily verifying the reliability of the sensor.

Furthermore, to fully exploit the self-powered characteristic of the sensor and achieve visual feedback of respiratory signals, a peak detection circuit is designed in this study. This circuit detects the peak voltage of the pulses output from the receiving coil and powers an LED. Thuse, the respiratory signal is synchronized with the on-off cycle of the LED. Fig. 7c shows a photograph of the signal processing circuit connected to the sensor and integrated into the waist belt, while Fig. 7d presents the schematic diagram of the signal processing circuit. The voltage signals at the LED port have been recorded when the subject is under three breathing modes, i.e., slow breathing, normal breathing, and breath holding (Fig. 7e). The voltage signal rates are about 10 and 19 beats per minute in the slow and normal breath stages respectively, which are fully consistent with the subject's breathing frequency. In addition, the node voltage successfully illuminated the LED, clearly and intuitively reflecting the respiratory rhythm (see Video 1). Fig. 7f illustrates the temporal correspondence between the voltage signal and the LED on-off cycle during normal breathing, further confirming the feasibility of this system for real-time, wireless, and intuitive visual respiratory detection.

In terms of joint motion detection, the sensor is attached to the skin surface over a volunteer's elbow or knee joint, with the receiving coil placed approximately 2 cm vertically from the device. When the elbow or knee is flexed for three times, the sensor is compressed, and the receiving coil immediately detects correspondingly three voltage pulse signals. The minimal peak-to-peak voltages are approximately 3.6 V and 3.0 V for elbow and knee motions respectively (Fig. 8). This result indicates that the sensor also possesses sensitive responsiveness to limb movements. Nevertheless, in practice the relative displacement between the sensor and the receiving coil—whether vertical separation or lateral offset—can exert a non-negligible influence on the output waveform. To mitigate this issue, resonant frequency detection can be employed as an alternative readout parameter to ensure measurement integrity (as suggested in Fig. 5c), while the deployment of multiple receiving coils effectively extends the tolerance range for horizontal displacement (Figure S4 in the Supplementary Information).

5. Conclusions

In summary, this work demonstrates the feasibility of piezoelectric-driven LC passive wireless sensing using a PVDF film. Theoretical simulations and experimental analyses have clarified how key design parameters, such as PVDF structural spacing and resonant antenna configuration, influence the amplitude and frequency of the output voltage. By adjusting the spacing layer and the resonant antenna structure, the proposed sensor can generate oscillatory signals with

tunable amplitudes and frequencies, thereby enhancing its adaptability to various practical scenarios. The sensor has been successfully applied to detect respiratory signal and joint movements, and it can power an LED using the mechanical energy of breathing. This favorable responsiveness to diverse physiological signals, together with its self-powered and wireless capabilities, demonstrates broad application prospects in fields such as health monitoring, motion analysis, and intelligent human-machine interaction.

CRediT authorship contribution statement

Heng Li: Visualization, Software, Data curation. **Rui Hu:** Validation, Software, Methodology. **Xuemei Lu:** Supervision, Funding acquisition. **Enting Gao:** Supervision, Funding acquisition. **Tao Peng:** Software, Methodology. **Baoqing Nie:** Writing – review & editing, Methodology, Funding acquisition, Formal analysis, Conceptualization. **Yaojun Yuan:** Writing – original draft, Validation, Investigation, Formal analysis, Data curation. **Donglin Wu:** Visualization, Software, Methodology, Data curation. **Jiaqi Zhang:** Visualization, Validation, Formal analysis.

Declaration of Competing Interest

The authors declare that they have no known competing financial interests or personal relationships that could have appeared to influence the work reported in this paper.

Acknowledgements

This work was supported by the National Natural Science Foundation of China (No. 62471326, No. 22203059), Jiangsu Key Laboratory of Biophotonics Open Projects Fund (Project No. 2025BPT003, 2025BPT004), Qing Lan Project.

Appendix A. Supporting information

Supplementary data associated with this article can be found in the online version at doi:10.1016/j.sna.2026.118418.

Data availability

Data will be made available on request.

References

[1] B.W. Lee, J. Kang, J.Y. Yoo, S.M. Won, Textile electronic systems for therapeutic applications, npj Flex. Electron. 9 (2025) 118.
[2] G. Yao, X. Gan, Y. Lin, Flexible self-powered bioelectronics enables personalized health management from diagnosis to therapy, Sci. Bullet. 69 (2024) 2289–2306.
[3] R.Z. Wu, T.X. Zhu, Y. Cheng, Z.K. Liu, J.Y. Huang, Y. Wei, et al., Materials, structure design, performances of multifunctional flexible devices for healthcare, Prog. Mater. Sci. 153 (2025) 101491.
[4] Z. Zhang, Y. Xu, Z. Zhang, S. Zhang, J. Liu, P. Zhang, et al., Strain-sensitive and strain-insensitive flexible electronics for healthcare monitoring, Adv. Healthc. Mater. 15 (2026) e03333.
[5] B.J. Chen, Z.M. Feng, F.Z. Yao, M.H. Zhang, K. Wang, Y. Wei, et al., Flexible piezoelectrics: integration of sensing, actuating and energy harvesting, npj Flex. Electron. 9 (2025) 58.
[6] Y.X. Dong, L.W. Duan, X.H. Mao, T. Gu, Y.Q. Gu, H.Y. Yu, et al., Exploring human motions for smart wearables: energy conversion, harvesting and self-powered sensing, Nano Energy 143 (2025) 111289.
[7] X. Wang, J. Huang, X. Jia, Y. Zhu, S. Xi, Self-powered flexible sensors: recent advances, technological breakthroughs, and application prospects, Sensors 26 (2025) 143.
[8] S. Zhang, S. Zhou, Z. He, O.O. Ibrahim, C. Liu, M. Wu, et al., Flexible epidermal sensor power systems: innovations in multidimensional materials and biomedical applications, Sensors 25 (2025) 3177.
[9] Y. Chen, T.Y. Wang, G.H. Gao, The principles and recent advancements in self-powered wearable fiber sensors, Mater. Chem. Front. 9 (2025) 1618–1649.
[10] R. Citroni, F. Mangini, F. Frezza, Efficient integration of ultra-low power techniques and energy harvesting in self-sufficient devices: a comprehensive overview of current progress and future directions, Sensors 24 (2024) 4471.
[11] M. Costanza, A.R.A. Laaraibi, A. Pagano, G. Jodin, F. Razan, I. Tinnirello, et al., Innovative battery-free wireless piezoresistive sensor for green-iot applications, Internet Things-Neth. 30 (2025) 101483.
[12] W. Yue, Y. Guo, J.C. Lee, E. Ganbold, J.K. Wu, Y. Li, et al., Advancements in passive wireless sensing systems in monitoring harsh environment and healthcare applications, Nanomicro Lett. 17 (2025) 106.
[13] Y.L. Wang, Y.P. Feng, X. Li, Z.B. Liu, C. Chen, D.Q. Cao, et al., Mutualistic symbiotic wireless node for next-era smart transportation, Nano Energy 136 (2025) 110746.
[14] H. Kim, B. Rigo, G. Wong, Y.J. Lee, W.H. Yeo, Advances in wireless, batteryless, implantable electronics for real-time, continuous physiological monitoring, Nanomicro Lett. 16 (2023) 52.
[15] R. Lin, H.J. Kim, S. Achavananthadith, S.A. Kurt, S.C.C. Tan, H. Yao, et al., Wireless battery-free body sensor networks using near-field-enabled clothing, Nat. Commun. 11 (2020) 444.
[16] E.Z. Lyu, Y.L. Sung, D.Y. Hsu, G.L. Su, T.W. Wang, Lc repeater-inspired battery-free, chipless, flexible body sensor network with lightweight reader, IEEE Trans. Instrum. Meas. 74 (2025) 1–11.
[17] J. Ma, H. Sun, Z. Chu, J. Zhao, Z. Yang, S. Liu, et al., Self-powered and self-calibrated sensing system for real-time environmental monitoring, Sci. Adv. 11 (2025) eadw3745.
[18] K.K. Wang, Y.M. Yao, Y.X. Liu, X. Guan, Y. Yu, J.L. Wang, et al., Self-powered system for real-time wireless monitoring and early warning of uav motor vibration based on triboelectric nanogenerator, Nano Energy 129 (2024).
[19] X. Dien, N. Ramli, T.H.G. Thio, Z. Yang, S. Hu, X. He, Energy storage, power management, and applications of triboelectric nanogenerators for self-powered systems: a review, Micromachines 16 (2025).
[20] K.X. Zhang, S.Z. Liu, S.S. An, Y. Zhou, X.J. Pu, Towards high-efficiency self-powered wireless sensor networks: a systematic review of co-design of energy and signal, Nano Energy 144 (2025).
[21] J. Si, J. Yang, R. Wang, K. Wang, Z. Wang, B. Wu, et al., Self-powered wireless sensing system based on triboelectric-discharge effect, IEEE Trans. Electron. Devices 71 (2024) 3874–3879.
[22] Y. Chen, X. Zhang, C. Lu, Flexible piezoelectric materials and strain sensors for wearable electronics and artificial intelligence applications, Chem. Sci. 15 (2024) 16436–16466.
[23] Y. Wang, M.L. Adam, Y. Zhao, W. Zheng, L. Gao, Z. Yin, et al., Machine learning-enhanced flexible mechanical sensing, Nanomicro Lett. 15 (2023) 55.
[24] V. Carluccio, L. Fachechi, V.M. Mastronardi, L. Natta, L. Algieri, G. de Marzo, et al., Fabrication, characterization, and signal processing optimization of flexible and wearable piezoelectric tactile sensors, IEEE Sens. J. 23 (2023) 10959–10969.
[25] Z. He, F. Rault, M. Lewandowski, E. Mohsenzadeh, F. Salaun, Electrospun pvdf nanofibers for piezoelectric applications: a review of the influence of electrospinning parameters on the beta phase and crystallinity enhancement, Polymers 13 (2021).
[26] M. Zhang, M. Li, W. Xu, F. Zhang, D. Yao, X. Wang, et al., Soft wireless passive chipless sensors for biological applications: a review, Biosensors 15 (2024).
[27] E. Markiewicz, J. Kulek, C. Pawlaczyk, Simple electric equivalent circuit method to determine piezoelectric and elastic properties of piezoelectric polymer film, IEEE T Dielect El 6 (1999) 304–308.
[28] Z.Y. Cao, Y. Chu, S.W. Wang, X.Y. Ye, Theoretical analysis of sensor properties of contact-separation mode nanogenerator-based sensors, Nano Energy 79 (2021) 105450.
[29] H.F. Zhao, H. Wang, H.Y. Yu, Q.H. Xu, X.S. Li, J. Guo, et al., Theoretical modeling of contact-separation mode triboelectric nanogenerators from initial charge distribution, Energ. Environ. Sci. 17 (2024) 2228–2247.
[30] W.H. Zhang, G.Q. Gu, H.X. Ren, Z.H. Zhang, Z.Y. Zhang, H.F. Qin, et al., A real-time self-powered wireless pressure sensing system based on capacitive triboelectric pressure sensor, Nano Energy 136 (2025) 110729.
[31] C. Chen, S. Zhao, C. Pan, Y. Zi, F. Wang, C. Yang, et al., A method for quantitatively separating the piezoelectric component from the as-received "piezoelectric" signal, Nat. Commun. 13 (2022) 1391.

Heng Li is a graduate student majoring in New Generation Electronic Information Technology at Soochow University. Her research focuses on flexible sensors based on wireless telemetry.

Yaojun Yuan was a master student in the School of Electronic and Information Engineering, Soochow University and received her master degree at 2026. Her research focuses on flexible, wearable sensing technology.

Donglin Wu is a graduate student majoring in New Generation Electronic Information Technology at Soochow University. His research focuses on wireless flexible sensors based on wireless telemetry.

Jiaqi Zhang is a graduate student majored in Information and Communication Engineering at the Soochow University. His research field is temperature sensing systems based on RFID wireless sensors.

Rui Hu is a graduate student majoring in New Generation Electronic Information Technology at Soochow University. Her research focuses on flexible sensors and the application in biomedical engineering.

Xuemei Lu is currently an associate professor at the School of Optics and Electronic Information of Suzhou City University. She received her Ph.D. degree from Soochow University in 2020. Her research interests are in electronic physics and biological physics.

Enting Gao is currently an associate professor of School of Electronic and Information Engineering, Suzhou University of Science and Technology. She received her Ph.D. degree from Soochow University in 2017. Her research interests are in data analysis based on machine learning.

Tao Peng is an Associate Professor in Soochow University. His main research interests include medical image processing, pattern recognition, machine learning, and their applications.

Baoqing Nie is an Associated Professor in School of Electronic and Information Engineering, Soochow University. Her research interests focus on flexible and stretchable sensing devices and the biomedical applications.